Modern Management Based on Big Data IV
A.J. Tallón-Ballesteros (Ed.)

doi:10.3233/FAIA230212

Numerical Investigation on Geomechanical Response and Well Performance in Shale Condensate Gas Reservoirs

Wentao LU[a], Yong ZENG[a], Mingming LIU[b, 1] and Lijun LIU[b]
[a] *Research Institute of Exploration and Development, Sinopec Jianghan Oilfield Company, Wuhan 430223, China*
[b] *Energy College, Chengdu University of Technology, Chengdu, 610059, China*

Abstract. Compared with conventional reservoirs, shale gas flow is greatly affected by matrix/fracture deformation, as well as nonlinear coupled transport mechanisms. In this paper, a hydro-mechanical coupled model is presented to describe the fluid flow in deformable shale formation. A unified compositional model is developed for modeling of multiphase fluid flow with phase transition. A series of mechanisms, including Knudsen diffusion, multi-component adsorption, confined phase behavior and molecular diffusion, are considered for accurate description of fluid flow in shale reservoirs. Matrix deformation is based on the linear poroelasticity theory. The fractures with complex geometry are modeled with the embedded discrete fracture model (EDFM). The mechanical responses of fractures are handled by different constitutive models, which are implemented into the coupled model. The flow and geomechanical models are spatially discretized using finite volume method (FVM) and finite element method (FEM), and the sequentially iterative approach is applied for solving the coupled model. Then the impacts of fracture orientation, in-situ stress condition, and bottom hole pressure on the mechanical deformation and gas production are investigated through sensitivity analysis. With multiple mechanisms and dynamic fracture behavior incorporated, the geomechanical response and well performance in shale condensate gas reservoirs can be accurately captured.

Keywords. Coupled flow and geomechanics; FEM; FVM; fracture network; shale condensate gas

1. Introduction

Over the last decade, shale resources have gained great attentions worldwide due to their large reserves. Hydraulic fracturing has been one of the most effective methods to improve hydrocarbon recovery from shale reservoirs [1]. Complex fracture networks can be generated when hydraulic fractures interact with the pre-existing natural micro-fractures [2]. Therefore, the formation can be divided into three components after hydraulic fracturing, which are matrix, micro-fractures, and hydraulic fractures.

[1] Mingming Liu, Energy College, Chengdu University of Technology, Chengdu, 610059, China; E-mail: woxinfeixiang1210@126.com.

Shale rocks are commonly characterized by nanoscale pores and abundant organic matters. These lead to several nonlinear fluid flow mechanisms, such as Knudsen diffusion and adsorption. Many efforts have been made to investigate the effects of these factors on fluid flow in shale reservoirs [3-5]. Among these studies, the hybrid model proposed by Lijun et al.[5] gives a comprehensive description of the multiple mechanisms, which include stress sensitivity, confined phase behavior, adsorption, and Knudsen diffusion. As the major flow conduits, fractures provide conductive pathways inside the formation, and bring a large portion of rock into direct contact with the well [6] . Meanwhile, fractures are highly sensitive to the mechanical loadings. Great aperture and conductivity lose may happen during depletion because of the increase of effective stress on fractures. However, the responses of hydraulic fractures and micro-fractures to the effective stress change are different. A lot of analytical and empirical hydraulic fracture conductivity models have been developed [7-9] Most empirical models depend on the experimental fittings, and the accuracy of predicting the proppant embedment and fracture conductivity may be not satisfactory in some cases. The analytical model derived with the contact mechanics give a unified description and good accuracy, such as Li's model [7]. Different from hydraulic fractures, micro-fractures are usually less propped, whose mechanical behavior mainly depends on its rough surfaces. The Barton-Bandis model [10, 11] is widely used to mimic the natural fracture deformation. Moinfar et al. [12] proposed a coupled flow and geomechanics model for fractured reservoir by introducing the EDFM and empirical joint models, but without the propped hydraulic fracture model. Jiang and Yang [13] developed a model for stress sensitive fractured shale reservoir with the nonlinear transport mechanisms and propped hydraulic fracture constitutive model, but lack of systematic analysis of the effect of fracture dynamic behavior.

In this study, a hydro-mechanical coupled model for shale condensate gas reservoirs is presented. A unified compositional model considering multiple mechanisms is developed for fluid flow in shale reservoirs. A linear elastic constitutive model coupled with propped hydraulic-fracture model and empirical natural-fracture model is used to model the mechanical deformation of matrix and fractures. The complex fracture network is handled by EDFM. Then sensitivity analysis is conducted to investigate the effects of fracture orientation, in-situ stress, and bottom-hole pressure on the shale gas production.

2. Numerical Model

Firstly, the shale condensate gas reservoir is discretized with structured grids. The complex network with hydraulic fractures and micro-fractures are efficiently modeled with EDFM. As shown in Fig 1, the orthogonal structured grids are applied for the matrix region, and fractures grids are generated by segmenting fractures with the matrix grid lines. Then the connectivity among these grids are extracted for the follow-up reservoir simulations.

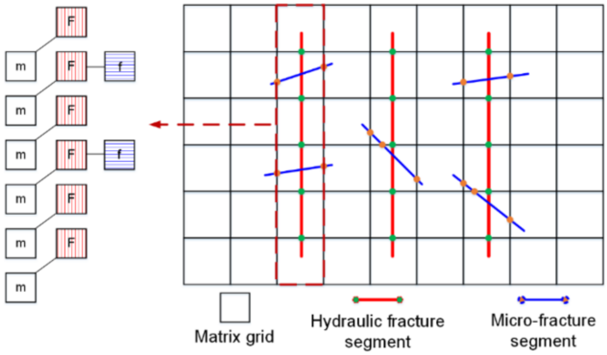

Fig 1. Schematic of shale condensate gas reservoir discretization: (left) grid connection and (right) grid structure.

For flow model, Eq. (1) is numerically discretized through FVM.

$$R_n^{i,t+1} = \frac{\{V[\phi(\rho_0 s_o x_i + \rho_g s_g y_i) + q_{ads,i}]\}_n^{t+1} - \{V[\phi(\rho_0 S_o x_i + \rho_g S_g y_i) + q_{ads,i}]\}_n^{t}}{\Delta t} - \sum_{m\in\eta_n} [(\rho_0 x_i \lambda_o)_{nm+\frac{1}{2}}^{t+1} \gamma_{nm}^{t+1}(\psi_{om}^{t+1} - \psi_{on}^{t+1}) + (\rho_g y_i \lambda_g)_{nm+\frac{1}{2}}^{t+1} \gamma_{nm}^{t+1}(\psi_{gm}^{t+1} - \psi_{gn}^{t+1})] - \sum_{m\in\eta_n} D_{eff,i} A_{nm}^{t+1} \frac{(\rho_g y_i)_m^{t+1} - (\rho_g y_i)_n^{t+1}}{d_n^{t+1} + d_m^{t+1}} - (Vq_i)_n^{t+1} \tag{1}$$

$$R_n^{w,t+1} = \frac{(V\phi\rho_w S_w)_n^{t+1} - (V\phi\rho_w S_w)_n^{t}}{\Delta t} - \sum\nolimits_{m\in\eta_n} \left[(\rho_w \lambda_w)_{nm+\frac{1}{2}}^{t+1} \gamma_{nm}^{t+1}(\psi_{wm}^{t+1} - \psi_{wn}^{t+1})\right] (Vq_w)_n^{t+1} \tag{2}$$

where η_n represents grids connected and n is grid block; $nm+1/2$ is the interface of grid blocks n and m; λ is phase mobility calculated as $\lambda_\beta = k_{r\beta}/\mu_\beta$; γ is the transmissibility calculated as

$$\gamma_{\rm nm} = \frac{A_{nm} K_{nm+1/2}}{d_n + d_m} \tag{3}$$

where A is the interface area, m^2; d is the vertical distances from cell center to interface, m.

The Newton-Raphson method is applied to solve the nonlinear Eqs. (2)-(3) with the following scheme

$$\sum_p \frac{\partial \mathrm{R}_n^{\beta,t+1}(x_{p,k})}{\partial x_p} \delta x_{p,k+1} = -\mathrm{R}_n^{\beta,t+1}(x_{p,k}) \tag{4}$$

$$x_{p,k+1} = x_{p,k} + \delta x_{p,k+1} \tag{5}$$

where x is the primary variable; p is the variable index; k is the iteration level.

For the geomechanical model, FEM is adopted for the numerical discretization. The weak form of Eq. (2) can be obtained as follows

$$\int_{\Omega}\delta\varepsilon:\sigma d\Omega = \int_{\Omega}\delta u \cdot \rho_b g\, d\Omega + \int_{\Gamma}\delta u \cdot \mathrm{T}_{ett}\, \mathrm{d}\Gamma \tag{6}$$

and Ω denotes the reservoir domain; Γ denotes the computational boundary with fixed traction; $\mathbf{T}_{\mathrm{ext}}$ is the exerted traction on boundary, Pa. The displacement vector $\boldsymbol{u}$ can be calculated with the nodal displacement $\bar{\boldsymbol{u}}$ and interpolation function $\boldsymbol{N}$

$$u = N\bar{u} \tag{7}$$

Substituting Eq. (7) into Eq. (6), the matrix-vector form of Eq. (7) can be obtained as follows

$$K\bar{u} = f \tag{8}$$

where

$$\boldsymbol{K} = \int_{\Omega}\boldsymbol{B}^T\boldsymbol{D}\boldsymbol{B}\mathrm{d}\Omega \tag{9}$$

$$\boldsymbol{Q} = \int_{\boldsymbol{\Omega}}\boldsymbol{\alpha p_t B^T m d\Omega} \tag{10}$$

$$\boldsymbol{f} = \int_{\Gamma}\boldsymbol{N}^T\boldsymbol{T}_{ext}\boldsymbol{d\Gamma} + \int_{\boldsymbol{\Omega}}\boldsymbol{N}^T\rho_b g\mathrm{d}\Omega \tag{11}$$

where $\boldsymbol{B} = \boldsymbol{LN}$; $\boldsymbol{L}$ is the matrix consisting with differential operators; **m** is delta Dirac function vector. The fixed-stress split method is applied for the solution of the coupled model due to its flexibility and stability[14], [15]. In one time step, the flow model is firstly solved by fixing the total mean stress, and then the updated fluid pressure is transferred to the solution of geomechanical model. The reservoir porosity and permeability update after the geomechanical problem is solved. This procedure repeats in one time step until the fluid pressure and rock deformation becomes stable, then the next time step begins. The flowchart of the solution procedure is shown in Fig 2.

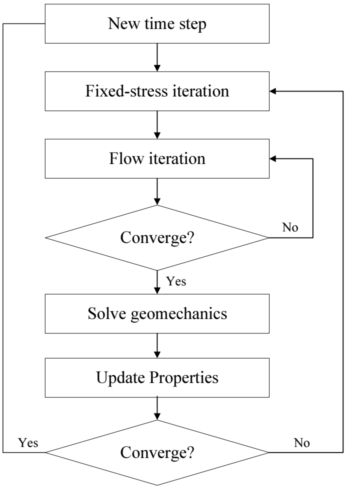

Fig 2. Flowchart of coupled flow and geomechanics problem.

3. Results and Discussions

A multi-stage fractured shale condensate gas reservoir model is used the parameters slightly modified from Roussel et al.[16]. The fluid properties and relative permeability curves in Liu et al.[5] are used. The reservoir and fracture geometry are shown in Fig 3, in which random micro-fracture networks are generated with the density of 0.08m/m^2. Table 1 shows the basic reservoir parameters for the base case.

Based on the reservoir model, the base case is simulated. Fig 4 shows the results of pressure and saturation distribution after 1500 days' depletion. The gas production results with and without consideration of geomechanics are given in Fig 5. It is clear that geomechanics has great influence on the gas production, and without considering geomechanics, the production may be greatly overestimated.

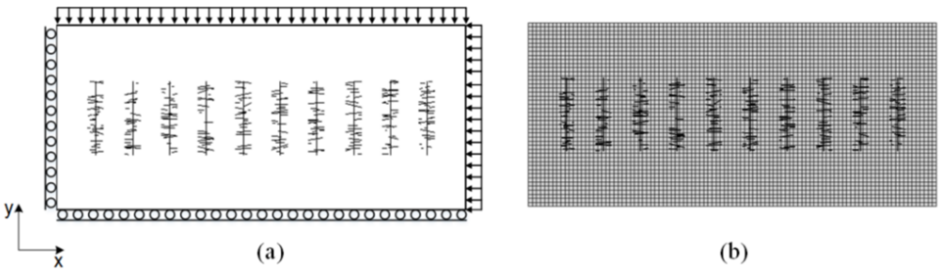

Fig 3. sketch for (a) fractured shale reservoir model and (b) computational grids.

Table 1. Details parameters.

Parameters	Value	Unit
Model dimension	1000×450×10	m
Grid size	10×10×10	m
Matrix porosity	0.1	–
Matrix permeability	6×10^{-4}	mD
Matrix Young's modulus	1.5×10^{4}	MPa
Matrix Poisson's ratio	0.7	–
Initial micro-fracture permeability	5×10^{3}	mD
Initial micro-fracture aperture	1×10^{-3}	m
Initial normal stiffness of micro-fracture	10^{4}	MPa
Maximum closure of micro-fracture	9×10^{-4}	m
Initial hydraulic fracture permeability	7×10^{4}	mD
Initial hydraulic fracture aperture	4×10^{-3}	m
Hydraulic fracture half-length	90	m
Hydraulic fracture spacing	90	m
Proppant Young's modulus	2×10^{4}	MPa
Proppant diameter	3×10^{-4}	m
Initial gas saturation	0.75	–
Initial reservoir pressure	36.03	MPa
Initial reservoir temperature	384.82	K
Well radius	0.1	m
Bottom hole pressure	10	MPa
In-situ stress in x-direction	75	MPa
In-situ stress in y-direction	75	MPa

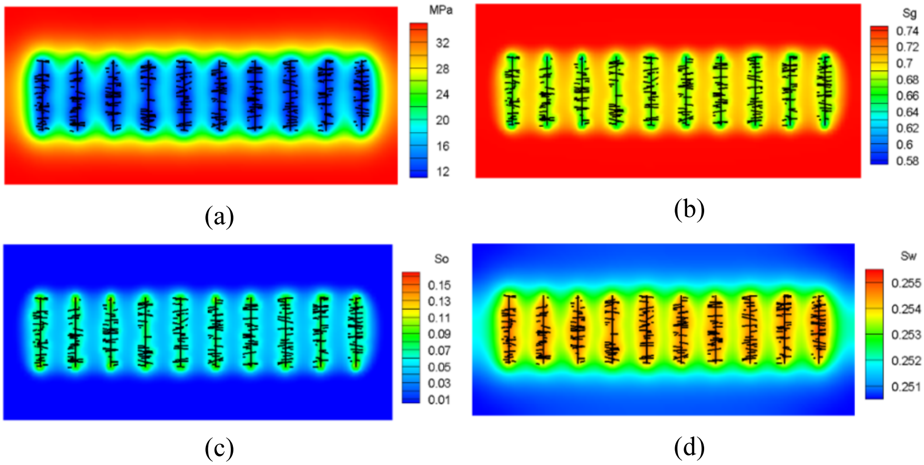

Fig 4. Simulation results of (a) pressure and saturations of (b) gas, (c) oil, and (d) water.

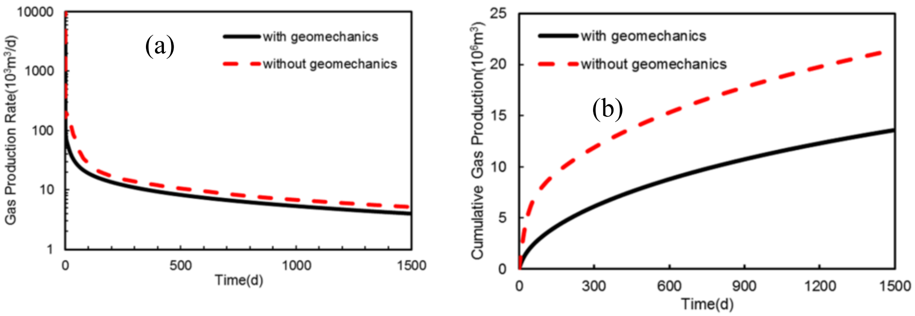

Fig 5. Curves for (a) gas production rate and (b) cumulative gas production with and without geomechanics.

3.1. Effect of Fracture Orientation

Different fracture orientations may occur when the horizontal wells are not drilled along the direction of the minimum principal stress. Therefore, it is necessary to study the dynamic behavior of fractures and gas production with different fracture orientations. With implementation of EDFM, complex fracture geometry can be handled in the simulation. Then different fracture orientations, consisting of 90˚, 60˚, and 30˚ angle of inclination, are investigated. Fig 6 shows the simulation results of pressure distribution. The gas production curves are given in Fig 7.

As shown in Fig 6, all the three cases have different drainage areas, in which the 90˚-inclination gives the largest depleted area, and 30˚-inclination has the least one. The size of depleted area commonly determines the production rate and gas recovery. As shown in Fig 7, as the fracture inclination decreases, the gas production decrease. But there is little difference between the gas production with 90˚-inclination and 60˚-inclination fractures because of the similar size of depleted area. Another observation from pressure distribution is that with the fracture inclination angle decrease, the distance among the fractures also decreases, which leads to the interference of neighboring fracture at late stage and explains why the gas production declines at late stage for the 30˚-inclination fractures.

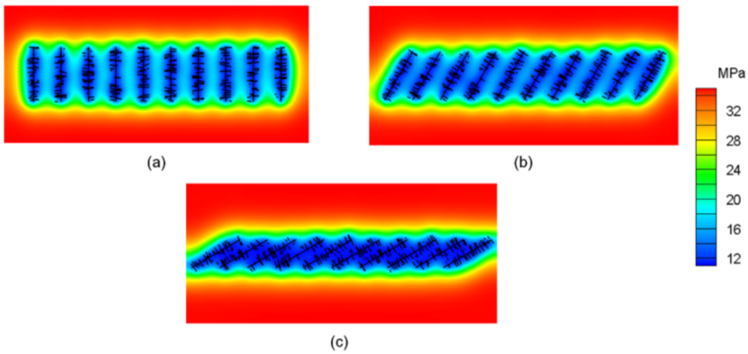

Fig 6 .Pressure distribution (a) 90˚, (b) 60˚, and 30˚.

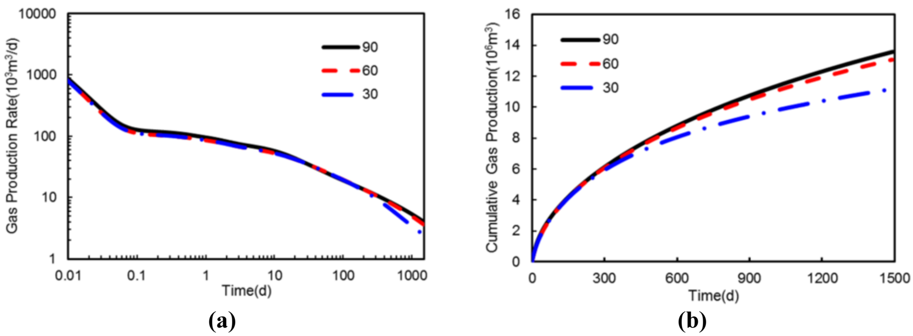

Fig 7. Curves for (a) gas production rate and (b) cumulative gas production with different fracture orientations.

3.2. In-Situ Stress

The effect of in-situ stress, here referring to the two horizontal principal stresses, on the gas production is investigated due to its important role in stress distribution and fracture aperture evolution. The x- and y-direction in-situ stress are analyzed separately, and take the values of 75MPa, which is a base case in the preceding subsections, as well as 55MPa and 35MPa. Fig 8 shows the hydraulic fracture aperture distribution with different x-direction in-situ stress, while the micro-fracture apertures show little difference and are not plotted. Similarly, Fig 9 shows the micro-fracture aperture distribution with different y-direction in-situ stress, and hydraulic fracture apertures are not given. Then the results of gas production are given in Fig 10.

The hydraulic fracture aperture changes, but little, with the x-direction in-situ stress, while the micro-fracture aperture is sensitive to the y-direction in-situ stress change which is shown in Fig 8 and Fig 9. The micro-fracture aperture with 35MPa y-direction in-situ stress is nearly twice of that with 75MPa y-direction in-situ stress. The directional effect of fracture aperture change is related to the normal directions of fracture surface. Obviously, in this case, the hydraulic fractures and micro-fractures are sensitive to the x- and y-direction in-situ stress, respectively. As for the different degree of change for hydraulic fracture and micro-fracture aperture, it is related with their different mechanical properties. The hydraulic fractures are stiffer due to the good propping of proppants rather than the weak rough surfaces. As a result, the gas production, shown in Fig 10, increases with the y-direction in-situ stress decreasing, while changes little with the y-direction in-situ stress. These results may guide the well drilling and completion that it is important to keep the micro-fracture networks suffering less stress.

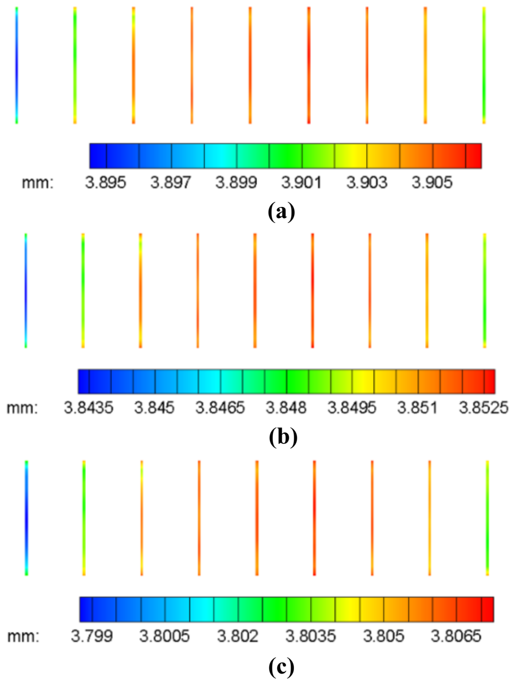

Fig 8 . Hydraulic fracture aperture with different x-direction in-situ stress of (a) 35, (b) 55, and 75MPa.

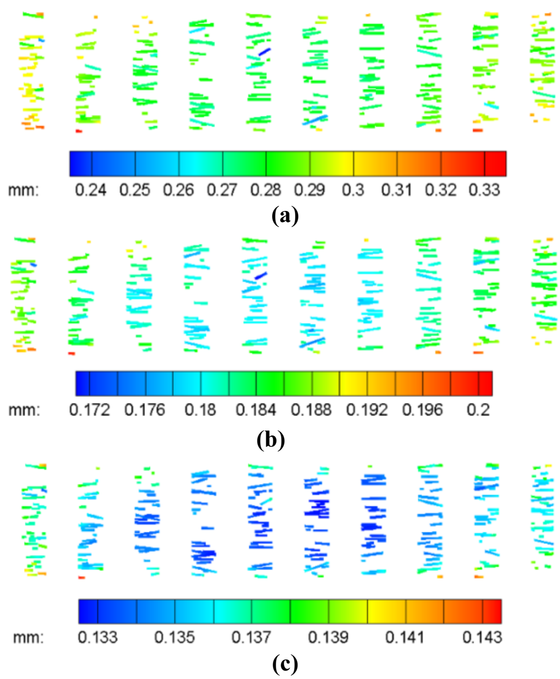

Fig 9. Micro-fracture aperture with different y-direction in-situ stress of (a) 35, (b) 55, and 75MPa.

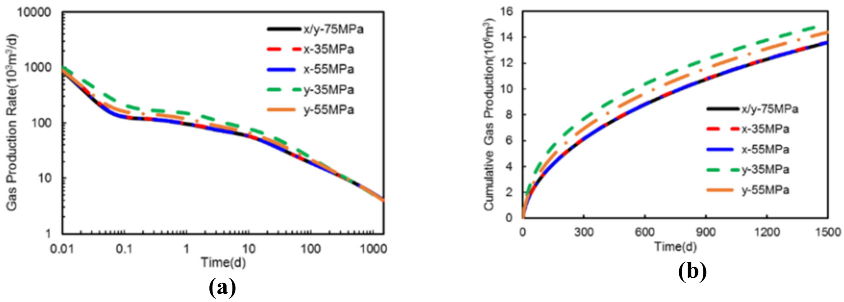

Fig 10. Curves for (a) gas production rate and (b) cumulative gas production with different in-situ stress.

4. Conclusions

A hydro-mechanical coupled model to simulate the geomechanical response and well performance in shale condensate gas reservoirs was developed in this work. A unified compositional model considering multiple mechanisms is implemented. The EDFM is adopted for efficient modeling of complex fracture geometry, and the mechanical response of micro-fractures and hydraulic fractures is handled by different constitutive models. Then the effects of fracture orientation, in-situ stress, and bottom-hole pressure on the gas production are investigated. The following conclusions drawing from the results are obtained:

1. Significant fracture aperture reduction and matrix deformation are obtained under geomechanical effect, and gas production can be greatly overestimated without considering this effect.
2. With the fracture inclination angle decreasing, the interference happens among fractures, leading to reduction in gas production.
3. The gas production is sensitive to the in-situ stress in the direction normal to micro-fracture because micro-fractures are more stress sensitive.
4. The gas production decreases greatly with the increase of bottom-hole pressure.

References

[1] Hubbert MK, Willis DG. Mechanics of hydraulic fracturing. Transactions of the AIME, 1957, 210(01): 153-168.
[2] Ahn CH, Chang OC, Dilmore R, Wang JY. A Hydraulic Fracture Network Propagation Model in Shale Gas Reservoirs: Parametric Studies to Enhance the Effectiveness of Stimulation. SPE/AAPG/SEG Unconventional Resources Technology Conference. OnePetro, 2014.
[3] Moridis GJ, Blasingame TA. and Freeman CM. Analysis of Mechanisms of Flow in Fractured Tight-Gas and Shale-Gas Reservoirs. SPE Latin American and Caribbean Petroleum Engineering Conference. 2010, Lima, Peru, Society of Petroleum Engineers: 22.
[4] Wu YS, Li J, Ding DY, Di Y. A generalized framework model for the simulation of gas production in unconventional gas reservoirs. Spe Journal, 2014, 19(05): 845-857.
[5] Lijun L, Jun Y, Hai S, Zhaoqin H, Xia Y, Longlong L. Compositional modeling of shale condensate gas flow with multiple transport mechanisms. Journal of Petroleum Science and Engineering, 2019, 172: 1186-1201.
[6] Shakiba M, Sepehrnoori K. Using embedded discrete fracture model (EDFM) and microseismic monitoring data to characterize the complex hydraulic fracture networks. SPE annual technical conference and exhibition. OnePetro, 2015.

[7] Li H, Wang K, Xie J, Li Y, Zhu S. A new mathematical model to calculate sand-packed fracture conductivity. Journal of Natural Gas Science and Engineering, 2016, 35: 567-582.
[8] Li K, Gao Y, Lyu Y,Wang M. New mathematical models for calculating proppant embedment and fracture conductivity. SPE Journal, 2015, 20(03): 496-507.
[9] Chen D, Ye Z, Pan Z, Zhou Y, Zhang J. A permeability model for the hydraulic fracture filled with proppant packs under combined effect of compaction and embedment. Journal of Petroleum Science and Engineering, 2017, 149: 428-435.
[10] Bandis S C, Lumsden A C, Barton N R. Fundamentals of rock joint deformation. International Journal of Rock Mechanics and Mining Sciences & Geomechanics Abstracts. Pergamon, 1983, 20(6): 249-268.
[11] Barton N, Bandis S, Bakhtar K. Strength, deformation and conductivity coupling of rock joints. International journal of rock mechanics and mining sciences & geomechanics abstracts. Pergamon, 1985, 22(3): 121-140.
[12] Moinfar A, Sepehrnoori K, Johns RT, Varavei A. Coupled geomechanics and flow simulation for an embedded discrete fracture model. SPE reservoir simulation symposium. OnePetro, 2013.
[13] Jiang J, Yang J. Coupled fluid flow and geomechanics modeling of stress-sensitive production behavior in fractured shale gas reservoirs. International Journal of Rock Mechanics and Mining Sciences, 2018, 101: 1-12.
[14] Kim J, Tchelepi HA, Juanes R. Stability and convergence of sequential methods for coupled flow and geomechanics: Fixed-stress and fixed-strain splits. Computer Methods in Applied Mechanics and Engineering, 2011, 200(13-16): 1591-1606.
[15] Dana S, Ganis B, Wheeler MF. A multiscale fixed stress split iterative scheme for coupled flow and poromechanics in deep subsurface reservoirs. Journal of Computational Physics, 2018, 352: 1-22.
[16] Roussel N P, Florez H A, Rodriguez A A. Hydraulic fracture propagation from infill horizontal wells. SPE annual technical conference and exhibition. OnePetro, 2013.